Journal of Solid State Chemistry 181 (2008) 3211–3216

Contents lists available at ScienceDirect

Journal of Solid State Chemistry

journal homepage: www.elsevier.com/locate/jssc

Crystal structure and lattice dynamics of $Sr_3Y(BO_3)_3$

M. Mączka [a,*], A. Waśkowska [a], A. Majchrowski [b], J. Kisielewski [c], W. Szyrski [c], J. Hanuza [d]

[a] Institute of Low Temperature and Structure Research, Polish Academy of Sciences, P.O. Box 1410, 50-950 Wrocław 2, Poland
[b] Institute of Applied Physics, Military University of Technology, 2 Kaliskiego Street, 00-908 Warszawa, Poland
[c] Institute of Electronic Materials Technology, Wólczyńska 133, 01-919 Warsaw, Poland
[d] Department of Bioorganic Chemistry, Faculty of Industry and Economics, University of Economics, ul. Komandorska 118/120, 53-345 Wrocław, Poland

ARTICLE INFO

Article history:
Received 20 June 2008
Received in revised form
12 August 2008
Accepted 17 August 2008
Available online 31 August 2008

Keywords:
Crystal structure
Phonon properties
Laser material
Borate

ABSTRACT

X-ray, Raman and infrared (IR) studies of the $Sr_3Y(BO_3)_3$ (BOYS) single crystal grown by the Czochralski technique are presented. The crystal structure is trigonal, space group $R\bar{3}$ (no. 148), and comprises six formula units in the unit cell with the hexagonal axes $a = 12.527(2)$ and $c = 9.280(2)$ Å. The assignment of the observed vibrational modes is proposed on the basis of lattice dynamics calculations. The unusual large bandwidth of the internal modes and the enhancement of the principal mean square thermal displacements for BO_3 and Y(1) indicate that some type of disorder is present in the studied crystal.

1. Introduction

Yb-doped materials, both crystals and glasses, are of great interest due to their potential applications in diode-pumped solid-state lasers. The simple electronic structure of Yb^{3+} ion eliminates unwanted effects such as excited-state absorption or upconversion. Moreover, small quantum defect limits the losses of the pumping power and the broad emission band allows the generation of femtosecond pulses. Therefore, Yb-doped materials can be used in high-power continuous wave lasers for material processing, as well as in femtosecond sources and tunable lasers in the near infrared (IR) [1]. One of the promising materials for Yb doping is the $Sr_3Y(BO_3)_3$ (BOYS) crystal [2–7]. It was shown, for instance, that Yb-doped BOYS crystal is a good candidate for femtosecond lasers fabrication: BOYS:Yb (20 at%) crystal was used in the construction of mode locked laser emitting 69 fs pulses at the central wavelength of 1062 nm [2].

Synthesis of strontium rare-earth borates described by the formula $Sr_3Ln(BO_3)_3$ (Ln = Y, Pr–Lu) was reported by Khamaganova et al. [5]. BOYS:Yb single crystals were grown using the Czochralski technique [6]. The crystal structure of BOYS was not resolved but it was reported that it is isostructural with $Sr_3Sc(BO_3)_3$ borate, which crystallizes in the $R\bar{3}$ structure [6,8]. The former studies revealed that phonon relaxations play an important role in the emission properties of this borate doped with Er^{3+} and Yb^{3+} [4]. Moreover, some bands observed in the emission and absorption spectra could be attributed to vibronic features [9,10]. However, phonon properties of this material are not known. Therefore, it is of interest to perform studies of the phonon properties of BOYS in order to understand spectroscopic features of the rare-earth ions in this matrix.

In this paper, results of X-ray diffraction, polarized Raman and IR studies as well as lattice dynamics (LD) calculations of the BOYS single crystal are reported. The experimental data along with the LD calculations give very accurate assignment of the observed modes and information on longitudinal optical (LO)–transverse optical (TO) splitting for this crystal.

2. Experimental

Single crystals of BOYS were grown using the Czochralski method. The thermal system consisted of a 53 mm outer diameter, 50-mm-high and 1.5-mm-thick iridium crucible, in passive iridium afterheater placed around the crucible top on the grog, and alumina heat shields around the afterheater. A charge material was prepared on the base of high purity (4.5 N) oxides and carbonate: Y_2O_3, B_2O_3, Yb_2O_3 and $SrCO_3$. After mixing, the charge material was heated at 1150 °C for 6 h in a resistivity furnace to obtain the BOYS compound. The growing atmosphere was pure nitrogen. The following conditions of the growth processes were applied: growth rate 0.6–1.2 mm h^{-1}; rotation rate 5–20 rpm; cooling after growth—at least 24 h. Firstly, single crystals were obtained by spontaneous nucleation on the

* Corresponding author. Fax: +48 71 344 1029.
E-mail address: m.maczka@int.pan.wroc.pl (M. Mączka).

0022-4596/$ - see front matter © 2008 Elsevier Inc. All rights reserved.
doi:10.1016/j.jssc.2008.08.025

Table 1
Crystal data and structure refinement parameters for BOYS

Formula weight	386.38
Temperature (K)	293(2)
Wavelength (Å)	0.71073
Crystal system, space group	Trigonal, $R\bar{3}$
Unit-cell dimensions (Å)	
a	12.5270(18)
c	9.2800(19)
γ (deg)	120
Volume (Å^3)	1261.2(4)
Z, calculated density (mg m^{-3})	6,4.173
Absorption coefficient (mm^{-1})	25.792
F (000)	1440
Crystal size (mm)	0.22 × 0.18 × 0.14
Γ Range for data collection	3.25–47.69
Limiting indices	$-21\leqslant h\leqslant 26$; $-16\leqslant k\leqslant 25$; $-12\leqslant l\leqslant 19$
Reflections collected/unique	9676/2517 [$R_{int} = 0.082$]
Completeness to $\Gamma = 47.31$	94.44%
Refinement method	Full-matrix least-squares on F^2
Data/restraints/parameters	2517/0/51
Goodness-of-fit on F^2	1.009
Final R indices [$I>2\sigma(I)$]	$R_1 = 0.0485$, w$R_2 = 0.0865$
Extinction coefficient	0.0092
Largest diff. peak and hole (e Å^{-3})	2.310 and −3.112

platinum wire. Then seeds cut off the crystals were used. The obtained single crystals up to 15 mm in diameter and 35–50 mm in length were free of macroscopic defects and inclusions of other phases. All the single-crystal boules were annealed in oxidizing atmosphere at 950 °C for 3 h, and then slowly cooled down to room temperature.

The single-crystal sample of dimensions given in Table 1 was selected for X-ray diffraction data collection with a four-circle diffractometer KM-4/CCD (Oxford Diffraction). The instrument was operated in κ geometry and used Mo$K\alpha$ radiation ($\lambda = 0.71073$ Å). The 1150 images were taken in nine runs with different angular settings and applying the ω-scan mode ($\Delta\omega = 1^\circ$ for each image, the exposure time was 25 s). Diffraction data were integrated for intensities and corrected for Lorentz-polarization effects using the *CrysAlis* program package [11]. The structure was solved by Patterson and electron density syntheses. The calculations were performed with the SHELX-97 program system [12].

Polycrystalline IR spectra were measured from the grounded crystals with a Biorad 575C FT-IR spectrometer in KBr suspension for the 1200–400 cm^{-1} region and in Nujol suspension for the 500–30 cm^{-1} region. Polarized IR spectra of a single crystal were measured in the $E||x$ and $E||z$ geometries at near normal incidence of 10° using a specular reflectance accessory. FT-Raman spectra were measured for an oriented single crystal using the BRUKER 110/S spectrometer with the YAG:Nd^{3+} excitation. Both IR and Raman spectra were recorded with a spectral resolution of 2 cm^{-1}.

3. Results

3.1. Structure determination

The BOYS compound is trigonal, space group $R\bar{3}$ (no. 148), and comprises six formula units in the unit cell with the hexagonal axes $a = 12.527(2)$ and $c = 9.280(2)$ Å. The crystal data, experimental details, and the structure refinement parameters are given in Table 1.

The structural motif consists of the strontium–oxygen polyhedron, two symmetrically distinct YO_6 octahedra, and the BO_3 triangle (Figs. 1 and 2). The atomic positional parameters are given in Table 2. The compound is isomorphous with $Sr_3Sc(BO_3)_3$ [8],

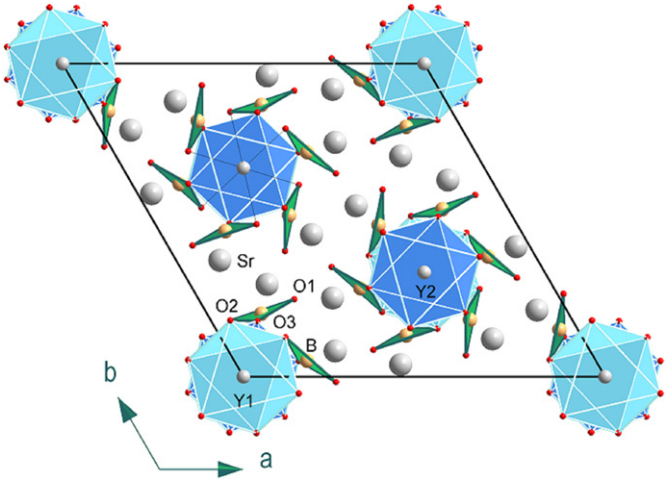

Fig. 1. View of the crystal structure of BOYS along the *c*-axis.

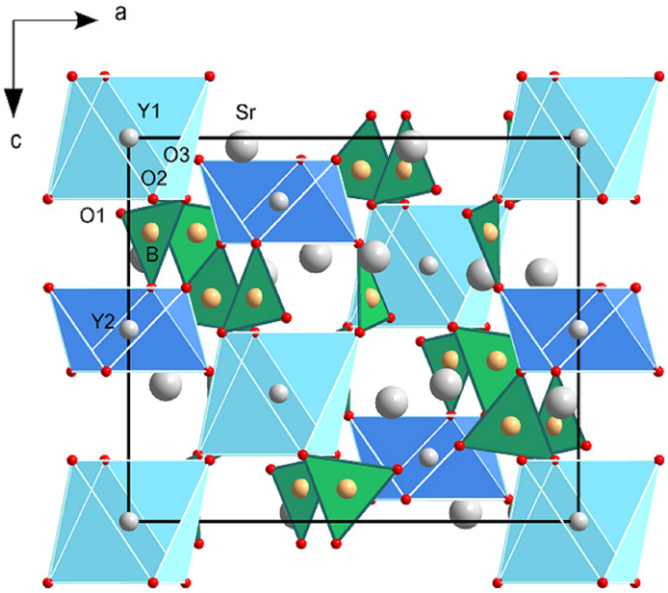

Fig. 2. View of the crystal structure of BOYS along the *b*-axis.

Table 2
Atomic coordinates ($\times 10^4$) and equivalent isotropic displacement parameters (Å $\times 10^3$) for BOYS

	X	Y	z	U_{eq}
Y(1)	0	0	0	19(1)
Y(2)	0	0	5000	51(1)
Sr(1)	1205(1)	3718(1)	233(1)	29(1)
B	1520(4)	2018(4)	2485(5)	20(1)
O(1)	539(4)	1808(4)	1619(6)	68(1)
O(2)	2658(4)	2487(3)	1982(5)	65(1)
O(3)	1284(5)	1784(4)	3911(4)	72(1)

U_{eq} is defined as one-third of the trace of the orthogonalized U_{ij} tensor.

but differs in details resulting from different covalent radii, R, of the Y and Sc-atoms. In the octahedral coordination, $R_{Sc} = 1.610$ and $R_Y = 1.780$ Å [13]. While in the Sc derivative, the Sr-atom exhibits nine-fold coordination, in the present structure the Sr-atom is an eight-fold coordinate (Table 3). The Y-atoms occupy two symmetrically independent Wyckoff positions 3*a*: (0,0,0) and

Table 3
Selected bond lengths (Å) and angles (deg)

B–O(1)	1.380(6)
B–O(2)	1.325(6)
B–O(3)	1.356(6)
Sr(1)–O(2)#1	2.439(4)
Sr(1)–O(1)	2.666(5)
Sr(1)–O(2)#3	2.524(4)
Sr(1)–O(1)#4	2.647(5)
Sr(1)–O(3)#2	2.680(5)
Sr(1)–O(2)#5	2.724(5)
Sr(1)–O(3)#4	2.894(5)
Sr(1)–O(3)#5	2.902(5)
Y(1)–O(1)	2.513(4) 6 ×
Y(2)–O(3)	2.238(4) 6 ×
O(2)–B–O(1)	122.5(5)
O(2)–B–O(3)	120.6(5)
O(1)–B–O(3)	116.7(4)

Symmetry transformations used to generate equivalent atoms: #1 $-x+1/3, -y+2/3, -z+2/3$; #2 $y-2/3, -x+y-1/3, -z+2/3$; #3 $-x+y-1/3, -x+1/3, z+1/3$; #4 $x+1/3, y+2/3, z+2/3$; #5 $x-y+1/3, x+2/3, -z+2/3$.

Table 4
Anisotropic displacement parameters ($Å^2 \times 10^3$) for BOYS

	U_{11}	U_{22}	U_{33}	U_{23}	U_{13}	U_{12}
Y(1)	16(1)	16(1)	24(1)	0	0	8(1)
Y(2)	16(1)	16(1)	119(1)	0	0	8(1)
Sr(1)	30(1)	26(1)	21(1)	−1(1)	2(1)	8(1)
B	28(3)	9(2)	27(3)	6(2)	11(2)	12(2)
O(1)	53(3)	56(3)	109(4)	−35(2)	−43(2)	37(2)
O(2)	42(2)	32(2)	96(3)	−12(2)	39(2)	0(2)
O(3)	126(4)	41(2)	38(2)	8(2)	15(2)	34(3)

The anisotropic displacement factor exponent takes the form $-2\pi^2[h^2a^2U_{11}+\cdots+2hkabU_{12}]$.

$3d$: $(0,0,\frac{1}{2})$, forming an octahedra with quite different configuration. The Y(1)–O_6 distances equal to 2.513(4) Å, while the Y(2)–O_6 distances are 2.238(4) Å. The O–Y–O angles indicate significant octahedral distortion since in the Y(1)O_6 they range from 87.92(2)° to 92.1(2)°, yet in Y(2)O_6 the distortion is even larger, as the octahedral angles run from 78.8(1)° to 101.2(1)°. The BO_3 triangles are not regular (Table 3). The average B–O distance 1.354(5) Å is shorter than in the Sc-containing structure with the corresponding bond equal to 1.38(1) Å.

The YO_6 octahedra are linked through the borate group into the chain with alternating Y(1) and Y(2) polyhedra running along the crystal c-axis (Fig. 2). Besides, the octahedron centered about Y(1) shares all vertices with the Sr-polyhedra, while in the Y(2)O_6 these are the faces common with the Sr-polyhedron. This diversity in linkages explains the elongation of the Y(1)–O and shortening of the Y(2)–O distances. By sharing corners, edges, and faces the Sr polyhedra form a three-dimensional framework, interconnected via borate groups with the YO_6 octahedra.

It is worth adding that some types of disorder (static or dynamic) in the present crystal cannot be excluded, since the principal mean square thermal displacements are enhanced for BO_3 and Y(1) (Table 4).

3.2. Raman and IR spectra

For the $R\bar{3}$ structure of BOYS group theory predicts $15A_g+15E_g+17A_u+17E_u$ Brillouin zone center modes. These modes can be subdivided into $2A_g+2E_g+2A_u+2E_u$ asymmetric stretching (ν_3), $A_g+E_g+A_u+E_u$ symmetric stretching (ν_1), $2A_g+2E_g+2A_u+2E_u$ in-plane bending (ν_4), $A_g+E_g+A_u+E_u$ out-of-plane bending (ν_2), $3A_g+3E_g+3A_u+3E_u$ translational and $3A_g+3E_g+3A_u+3E_u$ librational modes of the BO_3^{3-} groups. The remaining modes correspond to translations of the Sr^{2+} ($3A_g+3E_g+3A_u+3E_u$) and Y^{3+} ($2A_u+2E_u$) ions. It should be remembered, however, that among the translational modes, two modes (A_u and E_u) belong to the acoustic branches. The A_g and E_g modes are Raman active, and the A_u and E_u modes are IR active. This analysis shows that one expects to observe 30 modes in Raman and 32 modes in IR spectra.

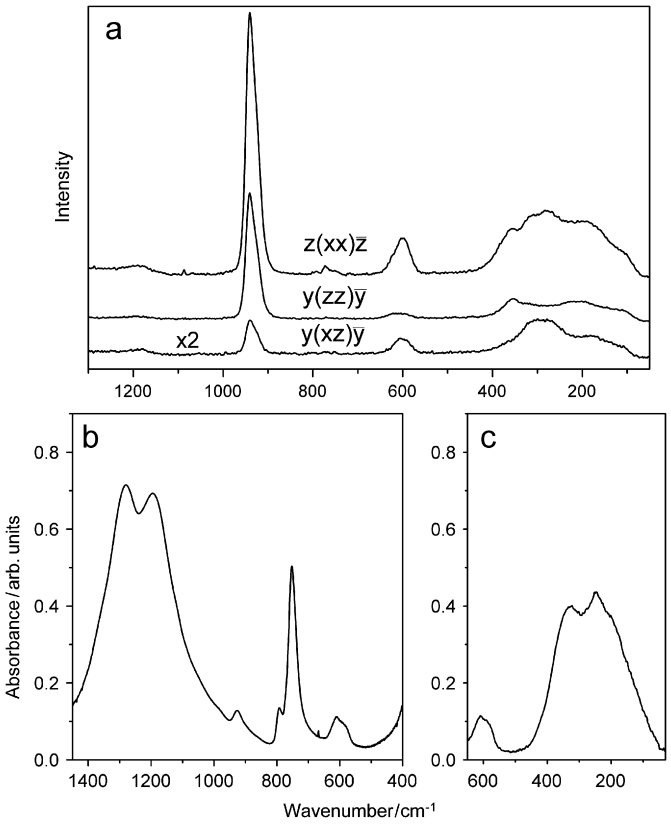

Fig. 3. Polarized Raman spectra (a) as well as polycrystalline IR spectra in the mid-IR (b) and far-IR (c) regions.

Room-temperature Raman spectra of the BOYS single crystal measured in different polarization configurations as well as the polycrystalline IR spectra are shown in Fig. 3. Fig. 4(a) presents the polarized IR spectra measured for the single crystal. These polarized IR spectra were fitted by using four parameters model in order to give information about TO and LO wavenumbers [14]. According to this model, the complex dielectric constant is expressed in terms of the IR-active modes as follows:

$$\varepsilon(\omega) = \varepsilon_\infty \prod_j \frac{\omega_{j\mathrm{LO}}^2 - \omega^2 + \mathrm{i}\omega\gamma_{j\mathrm{LO}}}{\omega_{j\mathrm{TO}}^2 - \omega^2 + \mathrm{i}\omega\gamma_{j\mathrm{TO}}} \quad (1)$$

where $\omega_{j\mathrm{TO}}$ and $\omega_{j\mathrm{LO}}$ correspond to the resonance wavenumbers of the jth transversal and longitudinal modes, respectively, and $\gamma_{j\mathrm{TO}}$ and $\gamma_{j\mathrm{LO}}$ are the corresponding damping factors. ε_∞ is the dielectric constant. For normal incidence, the IR reflectivity R and the dielectric function are related by

$$R = \left|\frac{\sqrt{\varepsilon}-1}{\sqrt{\varepsilon}+1}\right|^2 \quad (2)$$

The results of fitting of the experimental data to the four-parameter model are summarized in Table 5, where oscillator strengths $\Delta\varepsilon_{\mathrm{TO}}$ are also given. The plots of the calculated wavenumber dependence of the absorption coefficient and

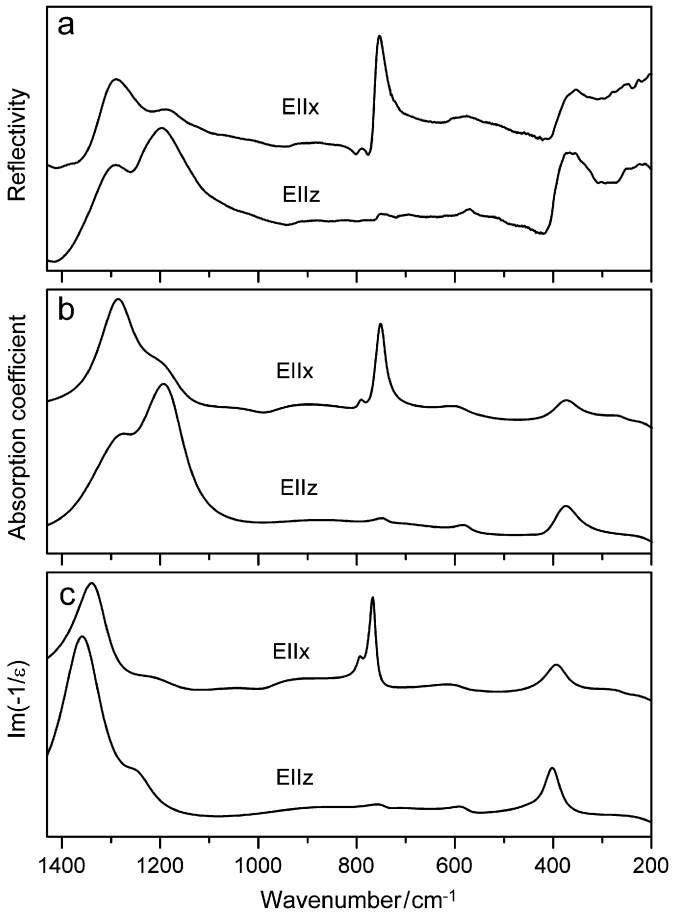

Fig. 4. Polarized reflection spectra (a), absorption coefficient (b) and imaginary part of the inverse dielectric function (c) for the BOYS crystal.

Table 5
Dispersion parameters for the best fit to the reflectivity data of BOYS for $E||x$ and $E||z$ polarization

ω_{TO} (cm^{-1})	γ_{TO} (cm^{-1})	ω_{LO} (cm^{-1})	γ_{LO} (cm^{-1})	$\Delta\varepsilon_{TO}$
$E||x$				
257.0	40.7	257.3	47.9	0.009
372.5	60.1	392.9	54.4	0.51
568.8	91.8	569.0	65.3	0.006
575.7	64.9	586.7	106.7	0.175
749.5	20.1	766.2	15.9	0.251
791.8	14.7	793.2	14.2	0.014
1178.8	96.0	1193.7	134.5	0.076
1279.3	67.6	1331.3	78.4	0.156
		$\varepsilon_\infty = 2.89$		
$E||z$				
373.6	57.0	401.6	39.7	0.127
577.8	38.1	580.4	41.6	0.023
740.5	31.6	740.7	34.8	0.002
756.0	115.3	757.2	101.5	0.014
1177.2	84.8	1245.3	75.7	0.500
1270.6	81.9	1357.1	100.7	0.089
		$\varepsilon_\infty = 2.86$		

imaginary part of the inverse dielectric function are presented in Figs. 4(b) and (c), respectively. The maxima of these plots correspond to TO and LO wavenumbers. Inspection of Table 5 shows that the largest LO–TO splittings, up to 86.5 cm^{-1}, are observed for the ν_3 modes.

Table 6
Potential parameters used for the lattice dynamics calculations

iTh ion	z_i (e)	a_i (Å)	b_i (Å)	C (kcal$^{1/2}$ Å^3 mol$^{1/2}$)
Sr	1.2	1.575	0.08	0
Y	1.35	1.378	0.09	0
B	1.5	0.429	0.08	0
O	−1.05	1.841	0.16	20
Ion pair	D_{ji} (kcal mol^{-1})	β_{ij} (Å)	r_{ij}^* (Å)	
B–O	26.0	2.72	1.44	

3.3. LD calculations

In order to adequately assign the Raman peaks to the atomic vibrations, we performed LD calculations. Since BOYS is mostly ionic, we performed the calculations on the basis of a partially ionic model described in the paper by Nozaki et al. [15]. The atomic positions used in the calculations were taken from the above-discussed X-ray structural studies. The following interatomic potential was used in the LD calculations:

$$U_{ij}(r_{ij}) = \frac{z_i z_j e^2}{r_{ij}} + (b_i + b_j)\exp\left[\frac{a_i + a_j - r_{ij}}{b_i + b_j}\right] - \frac{c_i c_j}{r_{ij}^6} + D_{ij}(\exp[-2\beta_{ij}(r_{ij} - r_{ij}^*)] - 2\exp[-2\beta_{ij}(r_{ij} - r_{ij}^*)]) \quad (3)$$

This interatomic potential consists of a Coulomb interaction (first term) to model the long-range interactions; a Born–Mayer-type repulsive interaction (second term) for accounting the short-range forces; a van der Waals attractive interaction (third term) to model the dipole–dipole interaction and finally the Morse potential contribution (last term) for taking into account the covalent bond character. z_i and z_j are the effective charges of the ions i and j, respectively, separated by the distance r_{ij}. The parameters (a_i, a_j) and (b_i, b_j) correspond to the ionic radii and ionic stiffness, respectively. The initial values of the parameters for the oxygen and boron were taken from Ref. [16]. The initial values of z and b parameters for Sr^{2+} and Y^{3+} were the same as those used for Ca^{2+} and Gd^{3+} in the LD calculations for $Ca_4GdO(BO_3)_3$ [16]. Since the parameters a reflect the radii, they were obtained for the Sr^{2+} and Y^{3+} ions using the values for the Ca^{2+} and Gd^{3+} reported in Ref. [16] and the expressions $a_{Sr} = a_{Ca}r_{Sr}/r_{Ca}$ and $a_Y = a_{Gd}r_Y/r_{Gd}$. The initial parameters were changed during the calculations in small steps in order to obtain the best agreement between the observed and calculated wavenumbers. The final parameters used in the present calculations are listed in Table 6. Since we consider covalency for the B–O bond only, D_{ij}, β_{ij} and r_{ij}^* are given for this bond. The calculated and experimental frequencies are shown in Table 7. The standard error of estimate of the calculated and experimental vibrational modes is 36.8 cm^{-1}.

4. Discussion

The former studies of borates showed that the internal modes of the planar BO_3^{3-} ion are observed around 900–1060 (ν_1), 650–800 (ν_2), 1200–1500 (ν_3) and 540–680 cm^{-1} (ν_4), respectively [16–19]. The present study is in agreement with the results obtained for other borates, showing that the wavenumbers of fundamental vibrations of the BO_3^{3-} ions are grouped into four distinct regions, i.e., 1323–1177, 943–926, 796–749 and 623–569 cm^{-1}. The polarization behavior of the Raman bands is not clearly observed, but our LD calculations help in assigning the modes to the respective symmetries, as proposed in Table 7. It is worth noting that in the 796–749 cm^{-1} region, three Raman bands

Table 7
Experimental and calculated vibrational modes of BOYS and their assignment

Raman					IR					Assignment
$z(xx)z$	$y(zz)y$		$y(xz)y$		Polycrystalline	$E\|\|x$		$E\|\|z$		
A_g+E_g	A_g		E_g			E_u		A_u		
Obs.	Calc.	Obs.	Calc.	Obs.	Obs.	Calc.	Obs.	Calc.	Obs.	
1298	1306	1323	1300	1281	1281	1295	1279	1307	1271	ν_3 (BO_3)
1189	1139	1191	1102	1184	1194	1133	1179	1104	1177	ν_3 (BO_3)
942+928	956	943	948	942+928	926	956		934		ν_1 (BO_3)
796					793					ν_2 (BO_3)
772+749	789		745		752	667	749	718	756	ν_2 (BO_3)
610	636	623	639	607	609	652	576	625		ν_4 (BO_3)
594	600	598	612	598	581	613	569	587	578	ν_4 (BO_3)
	415		412			416		417		T' (BO_3)
363	402		380	370		395	372	385	373	L (BO_3)
319	347	357	322	315	327	324		345		
279	272		281	270		284		321		
	252	224	255		246	256	257	258		
186	185	185	225	181	208	192		209		T' (Sr^{2+})
	125		153	142		181		163		
120	111	119	122			143		127		
	73		98							
						107		116		T' (Y^{3+})
						85		77		

are observed although only two are predicted by the group theory (A_g+E_g). Possibly, the extra band arises due to the Fermi resonance between the ν_2 modes and an overtone of a lattice mode. We cannot, however, exclude the possibility that the extra Raman band arises from the 749 cm^{-1} IR-active band, which becomes weakly active in the Raman scattering due to some disorder. It is worth to note that one additional band in this wavenumber region was observed by us previously also for $Ca_4GdO(BO_3)_3$ [16]. Another characteristic feature of the IR and Raman bands in the internal modes region is their large bandwidth. Former optical studies of BOYS doped with Yb^{3+} ions also showed that this borate exhibits a particularly broad zero-phonon absorption line, which enables efficient diode pumping of the crystal at 980 nm and tuning of the laser emission over a very large wavelength range (1020–1090 nm) [1,6]. This feature was assigned to the presence of two distinct sites occupied by Y^{3+} ions [9]. The presence of two Y^{3+} sites cannot, however, explain the observed large bandwidth for the internal modes of the BO_3^{3-} ions because these ions occupy only one site. Our results give, therefore, a strong argument that some type of disorder is present in the studied crystal. The Raman data support, therefore, the conclusion derived from the X-ray studies that some type of disorder in this crystal might be present.

Let us now discuss the origin of the bands observed below 400 cm^{-1}. These bands correspond to librational and translational motions of the BO_3^{3-} units, and translational motions of the Sr^{2+} and Y^{3+} ions. Factor group analysis predicts that there should be 18 Raman- and 20 IR-active modes in this region. It is worth adding that translational modes of the Y^{3+} ions are not active in the Raman spectra. Inspection of the spectra shows that the number of observed modes is much smaller than predicted. This result indicates that many modes have similar wavenumbers and are therefore not resolved in the room-temperature spectra. The former studies showed that translational modes of Ca^{2+} ions are observed in the 300–120 cm^{-1} region [16]. Since the atomic mass of Sr^{2+} ions is significantly larger than that of Ca^{2+}, the corresponding modes should be observed at lower wavenumbers. Our LD calculations indicate that the largest contribution of the translational motions of Sr^{2+} ions should be observed for the modes observed in the 208–142 cm^{-1} region. In a similar way, we may expect to observe the translational modes of the Y^{3+} ions at higher wavenumbers than the corresponding modes of the Gd^{3+} ions. The comparison of the spectra with the results obtained for $Ca_4GdO(BO_3)_3$ and $NdFe_3(BO_3)_4$, for which translations of Gd^{3+} and Nd^{3+} were located below 120 cm^{-1} [16,20] shows that these modes should be observed below 160 cm^{-1}. Our LD calculations are in agreement with this assumption since they show the largest contribution from translational motions of the Y^{3+} ions is expected for the two lowest wavenumber IR modes (see Table 7). However, the corresponding IR bands are probably very weak and cannot be clearly seen due to overlapping with much stronger and very broad bands observed at higher wavenumbers. The remaining bands below 400 cm^{-1} can be assigned to the lattice vibrations of the BO_3^{3-} ions. These modes are strongly coupled but our LD calculations suggest that the higher wavenumber modes have larger contribution of the translational motions and the lower wavenumber modes have larger contribution of the librational motions.

5. Conclusions

X-ray structural studies revealed that the Y-atoms, substituting Sc in $Sr_3Sc(BO_3)_3$ compound, caused distinct shifts of the BO_3 groups located in the general Wyckoff positions (18*f*). Consequently, in the BOYS structure, the oxygen sublattice becomes substantially distorted and the polyhedral distortions are significantly larger than in the Sc derivative.

The performed Raman and IR studies and the performed LD calculations allowed us to establish symmetries of the observed vibrational modes and propose assignment of the observed modes to the respective vibrations of structural units. They also confirmed the conclusion obtained from the crystallographic studies that some type of disorder (static or dynamic) is present in this crystal.

References

[1] S. Chénais, F. Druon, F. Balembois, P. Georges, R. Gaumé, P.H. Haumesser, B. Viana, G.P. Aka, D. Vivien, J. Opt. Soc. Am. B 19 (2002) 1083.
[2] F. Druon, S. Chénais, P. Raybaut, F. Balembois, P. Georges, R. Gaumé, G. Aka, B. Viana, S. Mohr, D. Kopf, Opt. Lett. 27 (2002) 197.
[3] R. Gaumé, B. Viana, D. Vivien, J.P. Roger, D. Fournier, J.P. Souron, G. Wallez, S. Chénais, F. Balembois, P. Georges, Opt. Mater. 24 (2003) 385.
[4] D. Zhao, Z. Hu, Z. Lin, G. Wang, J. Cryst. Growth 277 (2005) 401.

[5] T.N. Khamaganova, N.M. Kuperman, Zh.G. Bazarova, Russ. J. Inorg. Chem. 41 (1998) 1100.
[6] P.H. Haumesser, R. Gaumé, J.M. Benitez, B. Viana, B. Ferrand, G. Aka, D. Vivien, J. Cryst. Growth 233 (2001) 233.
[7] R. Ebothé, I.V. Kityk, J. Kisielewski, T. Lukasiewicz, R. Diduszko, A. Majchrowski, Appl. Phys. Lett. 89 (2006) 131106.
[8] P.D. Thompson, D.A. Keszler, Chem. Mater. 6 (1994) 2005.
[9] R. Gaumé, P.H. Haumesser, E. Antic-Fidancev, P. Porcher, B. Viana, D. Vivien, J. Alloy. Compds. 341 (2002) 160.
[10] P.H. Haumesser, R. Gaumé, B. Viana, E. Antic-Fidancev, D. Vivien, J. Phys. Condens. Matter 13 (2001) 5427.
[11] *CrysAlis* CCD and *CrysAlis* RED. Issue 171.32.6, Program System for Data Collection and Data Reduction, Oxford Diffraction Ltd., Wrocław, Poland, 2007.
[12] G.M. Sheldrick, *SHELXS* 97 and S*HELXL* 99 Programs for the crystal structure solution and crystal structure refinement, University of Gottingen, 1997.
[13] G.M. Sheldrick, Acta Crystallogr. A 64 (2008) 112.
[14] F. Gervais, P. Echegut, in: R. Blinc, P. Levanyuk (Eds.), Incommensurate Phases in Dielectrics, North-Holland, Amsterdam, 1986, p. 337.
[15] R. Nozaki, J.N. Kondo, C. Hirose, K. Domen, A. Wada, Y. Morioka, J. Phys. Chem. B 105 (2001) 7950.
[16] M. Mączka, J. Hanuza, A. Pajączkowska, Y. Morioka, J.H. Van der Maas, J. Raman Spectrosc. 35 (2004) 266.
[17] H.R. Xia, L.X. Li, J.Y. Wang, W.T. Yu, P. Yang, J. Raman Spectrosc. 30 (1999) 557.
[18] X.B. Hu, J.Y. Wang, C.Q. Zhang, X.G. Xu, C.-K. Loong, M. Grimsditch, Appl. Phys. Lett. 85 (2004) 2241.
[19] D. Fausti, A.A. Nugroho, P.H.M. Loosdrecht, S.A. Klimin, M.N. Popova, L.N. Bezmaternykh, Phys. Rev. B 74 (2006) 24403.
[20] A. de Andres, F. Agullo-Rueda, S. Taboada, C. Cascales, J. Campa, G. Ruiz-Valero, I. Rasines, J. Alloy. Compds. 250 (1997) 396.